processes

MDPI

Article

Effects of Layering Angle and Prestress on Dynamic Load Energy Conversion and Damage Mechanism of Sandstone

Wenbing Fan [1], Junwen Zhang [1,*], Yang Yang [2], Kailun Fang [3], Shaokang Wu [1] and Yulong Xing [4]

[1] School of Energy and Mining Engineering, China University of Mining and Technology (Beijing), Beijing 100083, China; bqt2000101024@student.cumtb.edu.cn (W.F.); gqt2200101006@student.cumtb.edu.cn (S.W.)
[2] China Center for Safety Research, Ministry of Emergency Management of the People's Republic of China, Beijing 100013, China
[3] Guangzhou Urban Planning and Design Co., Ltd., Guangzhou 510030, China
[4] Hebei Haowei Xuguang New Material Technology Co., Ltd., Handan 057350, China; bqt1900101015@student.cumtb.edu.cn
* Correspondence: zhangjw@cumtb.edu.cn

Abstract: Previously conducted studies have established the conversion relationship between incident energy, reflected energy, transmitted energy and absorbed energy of rocks under dynamic load. In this paper, the combined dynamic and static loading tests of sandstone under different prestress and different bedding angles are carried out to explore the law of the influence of prestress and bedding angles on energy evolution and damage evolution. The purpose is to provide some reference for deep mining, rock engineering design and geological hazard assessment. The energy conversion and damage characteristics of sandstone in the whole process of deformation are studied, and the internal energy conversion mechanism of sandstone under dynamic load is proposed. It is found that the increase in prestress will lead to the increase in the initial energy value of sandstone and further affect the shape of the energy evolution curve. In addition, the relationship between strain and energy transformation is established, and it is found that the energy transformation in different stages is different. At the same time, the relationship between prestress and damage characteristics and bedding angle and damage characteristics is established, and it is found that bedding angle and prestress significantly affect the damage characteristics.

Keywords: layered sandstone; mining application; internal energy conversion; failure mechanism; damage mechanism; phased energy characteristics

Citation: Fan, W.; Zhang, J.; Yang, Y.; Fang, K.; Wu, S.; Xing, Y. Effects of Layering Angle and Prestress on Dynamic Load Energy Conversion and Damage Mechanism of Sandstone. *Processes* **2023**, *11*, 2641. https://doi.org/10.3390/pr11092641

Academic Editor: Adam Smoliński

Received: 1 August 2023
Revised: 23 August 2023
Accepted: 30 August 2023
Published: 4 September 2023

1. Introduction

In geological processes, the interplay of sedimentation, changes in sedimentary environments, sediment characteristics and geological deformation can lead to the development of distinct layered structures in multiple orientations [1]. These structural interactions give rise to typical stratified rocks within rock layers, making the investigation of their mechanical properties a focal point in the realm of rock mechanics [2–4]. As depicted in Figure 1, underground engineering involves both dynamic and static loads affecting the surrounding rock [5–10]. Nevertheless, a comprehensive study on the energy conversion and damage mechanisms induced by dynamic loads, with consideration to bedding angle and prestress, remains lacking. As such, this research aims to thoroughly explore the influence of bedding angle and prestress on the dynamic load energy conversion and damage mechanisms in sandstone. The findings from this study will yield a comprehensive comprehension of sandstone's energy conversion and damage mechanisms, which holds significant implications for deep mining, rock engineering design and geological hazard assessment.

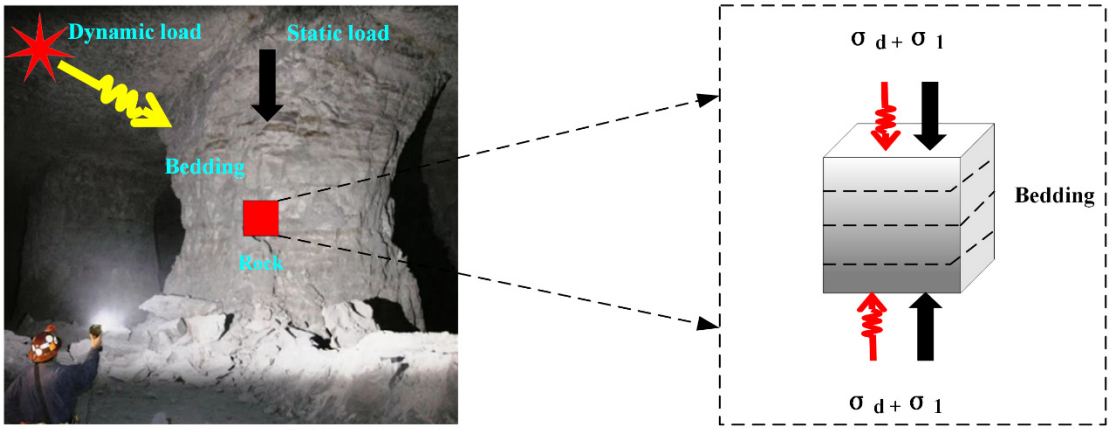

Figure 1. Load state of surrounding rock inside pillar.

A lot of research has been conducted on underground safety operations in coal and metal mines, for example, Khayrutdinov M.M. puts forward a different method to evaluate the state of rock mass, which is a good improvement on the current state assessment of rock mass. It provides a new way of thinking for mining [11]. Adigamov A.E proposed a new mathematical model which takes into account the stress–strain state of anisotropic disturbed rock mass. This paper provides some reference for underground engineering safety operation. In addition, disturbance will also affect the state of rock mass after mining [12]. Rybak, J.M. established the sequence of disturbance development and proposed methods to reduce the impact of underground mining on destructive bodies. This study has great significance for mining disturbance [13]. Kongar-Syuryunthe, Ch proposed a methodology of selecting a mineral deposit development technology. It provides a certain reference for safe mining [14]. In terms of the study of rock dynamic loading behavior and energy characteristics, Chang used a static and dynamic test system to conduct a static fracture comparison test on NSCB samples. It was found that the fracture paths of NSCB samples were different with different loading rates [15]. Zhao conducted fracture tests on coal samples. Their study revealed that the fracture toughness differed significantly depending on the bedding angle [16]. Zhang conducted dynamic impact tests on sandstone and found that the tensile cracks of sandstone increased with high loading levels [17]. Ye conducted dynamic impact tests on graphitic rock and obtained the law that the softening coefficient decreases and the hardening coefficient is proportional to the impact rate [18]. Wu found that the fracture modes of intact specimens and those with open porosity were significantly different. At the same time, the presence of pre-porosity would significantly degrade rock parameters [19]. Lu studied the brittle–toughness characteristics of sandstone. The relationship between water content and strength was observed, and sandstones with varying water content exhibited distinct microscopic mechanisms [20]. Liu designed a true triaxial impact rock burst test, and the study found that the degree of rock breakage varies with different loading methods [21]. Cen found that the dynamic load frequency was positively correlated with the unloading modulus of sandstone; in addition, the cyclic dynamic impact tensile strength was greater than the cyclic static impact tensile strength [22,23]. Zho conducted dynamic load tests on 3D created rocks and found that the crack growth modes of rocks under dynamic load and static load impacts are different [24]. Wu conducted dynamic load impact tests on jointed rock and observed that the strength of the intact specimen surpassed that of the jointed specimen [25]. Yan investigated the behavior of parallel fractured sandstone under dynamic load impact. The results show that there is a significant correlation between strain rate and rock deformation [26,27]. Li found that there was no obvious rule between the impact pressure and the elastic modulus [28]. Li found that the existence of prefabricated cracks affects the dynamic strength characteristics of coal [29]. In terms of the study on the mechanical behavior and energy characteristics of rock under dynamic and static combined loading, tao found that prestress and dynamic disturbance caused strong

instability and failure of rock, which was verified by numerical simulation [30]. Chang found that the increase in impact velocity strengthens the difference [31]. Wang's study revealed notable differences in the particle size of coal samples under distinct loading methods [32]. Zhou's research demonstrated how prestress influenced the failure mode of sandstone [33]. Li's investigation, using self-developed test equipment, focused on studying the fracture process of pre-cut sandstone specimens. The study revealed that rock damage under static load is caused by stress concentration and far-field strain around the pre-cut hole [34]. Cai found that saturated sandstone exhibits small pre-peak energy consumption and more post-peak energy dissipation [35]. Ke found that the freeze–thaw cycle changes the pattern of rock failure [36]. Du's research demonstrated that the presence of confining pressure changes the failure pattern of rock [37,38]. Zhu's work explored the different energy evolution modes of sandstone under various prestresses [39].

Analyzing the above, it can be noted that the study of rock mechanical behavior under impact loads is a very topical issue. Therefore, the purpose of this study is to explore the impact of the underlying bedding angle of impact load and prestress on the energy conversion and damage mechanism of sandstone. The findings from this study will yield a comprehensive comprehension of sandstone's energy conversion and damage mechanisms, which holds significant implications for deep mining, rock engineering design and geological hazard assessment. To achieve this, it is necessary to solve the following tasks: (1) the combined dynamic and static loading test of sandstone under impact load; (2) the global energy evolution curve and damage mechanism curve of sandstone under an impact load are calculated based on the energy calculation principle.

2. Test Plan

2.1. Sample Preparation

The sandstone samples utilized in this study were obtained from Jixi City, Heilongjiang Province. In Figure 2, the sandstone exhibits a gray appearance, likely attributed to its unique mineral and particle composition. Moreover, the presence of a distinct bedding structure is evident, clearly delineating layers within the rock. The formation of this bedding structure is likely linked to the historical processes of rock deposition and deformation. For the dynamic and static combined loading tests, a series of 50 mm × 50 mm cylindrical samples were extracted from the same parent rock. These tests were conducted with varying prestresses and bedding angles. Furthermore, XRD and SEM analyses were carried out to gain comprehensive insights into the sandstone's microstructure, mineral composition and intergranular relationships. The XRD test equipment used in this paper is the Dutch Panaco brand, and the model number is X'Pert. In the SEM test, we used the German ZEISS test equipment, and the model number is GeminiSEM 300. In addition, the Inorganic Crystal Structure Database (ICSD) was used for XRD: this database contains structural information on inorganic compounds, including X-ray data, unit cell parameters and atomic coordinates. In the XRD test preparation process, first, the sample is pulverized using tools such as a mortar and pestle to obtain sufficiently fine particles (about 45 μm in diameter). This helps to reduce the crystal size and improve the resolution of XRD tests. In the SEM test, the sandstone is cut into thin sheets or a part of it is removed and then polished to obtain a smooth surface. In addition, due to the poor electrical conductivity of sandstone, we gold-plated the cut rock to improve the electrical conductivity of sandstone, making the SEM image of sandstone more clear. At the same time, in the SEM test, we used a Soper brand drying oven to dry SEM samples of sandstone; after our measurement, the initial humidity of the sandstone before drying was 0.04%, and the final humidity of the sandstone after drying was 0.01%. This is because thorough drying will cause certain damage to the rock, so we only partially dried the sandstone. The XRD and SEM results confirm the sandstone's composition as sandstone, further highlighting the significant bedding effect.

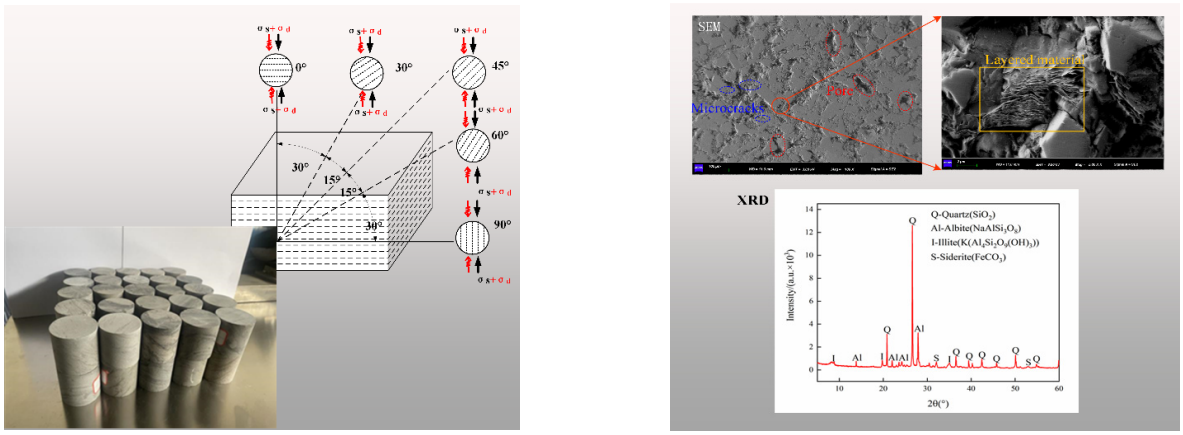

Figure 2. Typical rock sample.

2.2. Test Scheme and Dynamic Stress Balance

To explore the energy evolution and damage mechanism of sandstone, we conducted a series of carefully designed experiments. First, the sandstone samples were initially loaded with different prestressing levels (0 MPa, 12.5 MPa, 25 MPa, 37.5 MPa and 50 MPa). In addition, the angle of application of stress to the test sample is shown in Figure 3a. This means that the angle of stress application is constant. The selected prestress levels were specifically chosen to mimic various stress conditions commonly encountered in practical engineering, thereby facilitating a deeper comprehension of sandstone's energy and damage mechanisms. Following the initial loading, we proceeded with dynamic impact tests on the sandstone samples, encompassing 5 distinct angles (0°, 30°, 45°, 60°, 90°). These angles were deliberately selected to investigate how sandstone responds under different bedding conditions. By applying shock loads to the test, we can simulate shock loads in geological disasters, such as earthquakes or explosions. Furthermore, the experimental setup involved the utilization of improved SHPB equipment to conduct this test (as depicted in Figure 3a). Ensuring dynamic stress balance during this test is of paramount importance. In this regard, Figure 3b demonstrates the dynamic stress balance observed in typical sandstone. The figure clearly indicates that the sandstone conforms to the dynamic stress balance requirements, thereby validating the integrity and reliability of the test data presented in this study.

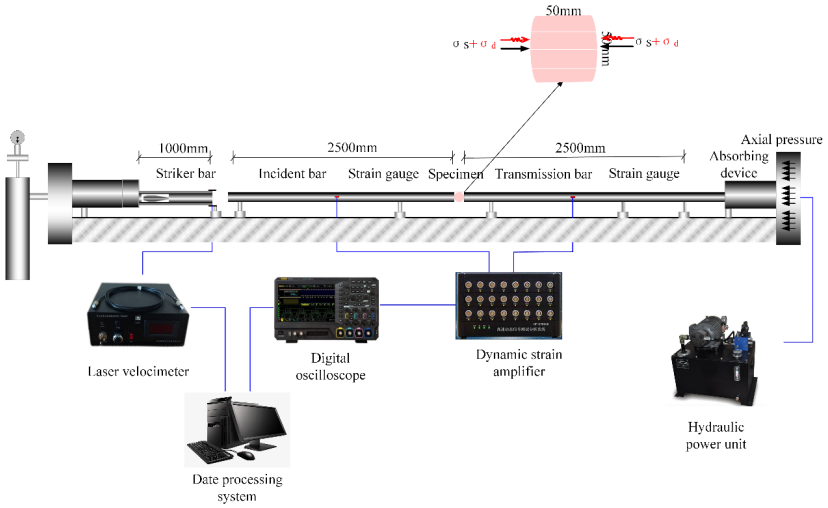

(**a**)

Figure 3. *Cont.*

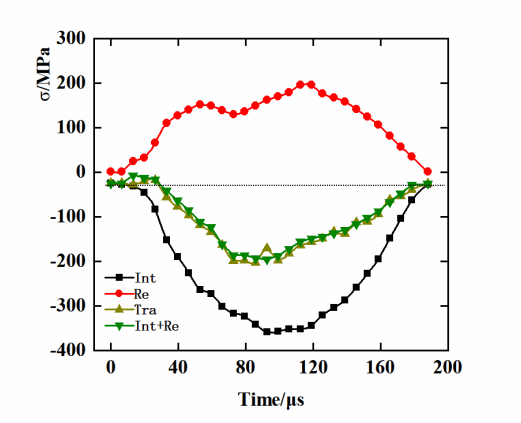

(**b**)

Figure 3. Improved SHPB and dynamic stress balance. (**a**) Improved SHPB; (**b**) dynamic stress balance.

3. Principle of Energy Calculation

Studying the transfer laws of elastic and dissipative energy in sandstone during combined dynamic and static loading tests under varying prestress and bedding angles holds significant importance. Such understanding is crucial for comprehending the mechanical response and damage mechanisms of rocks. As depicted in Figure 4, the calculation of the total energy U of sandstone under different prestress and bedding angles is as follows [40–43]:

$$U = U^{e} + U^{d} \tag{1}$$

where U^{e} represents the elastic energy and U^{d} stands for the dissipative energy of sandstone. During this experiment, the U, U^{e} and U^{d} of the sandstone conform to the following formulas:

$$U = \int_{0}^{\varepsilon_1} \sigma_1 d\varepsilon_1 \tag{2}$$

$$U^{e} = \frac{1}{2}\sigma_1\varepsilon_1^{e} = \frac{1}{2E_u}\sigma_1^2 \tag{3}$$

$$U^{d} = U - U^{e} \tag{4}$$

where σ_1 represents the axial principal stress, ε_1 denotes the axial principal strain and E_u corresponds to the corresponding elastic modulus.

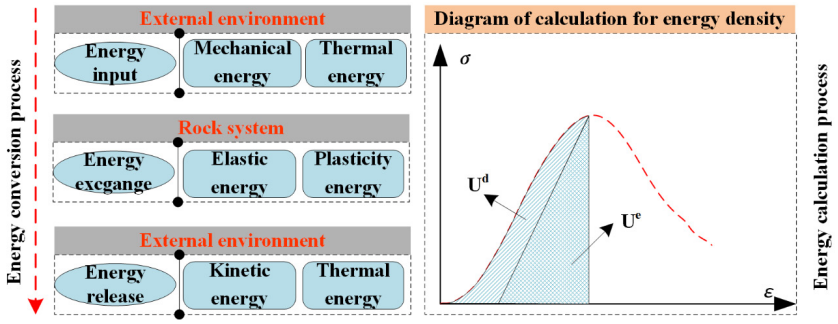

Figure 4. Energy calculation method of rock.

4. Global Energy Conversion Characteristics of Sandstone

The test of sandstone under varying prestress and bedding angles yields distinct global energy evolution patterns, attributed to the influence of prestress and bedding angle. Figure 5 illustrates the global energy evolution of sandstone under these conditions. This evolution is categorized into five stages: Stage I, the static loading stage (absent when

sandstone is tested under pure dynamic loading); Stage II, the secondary pressure sealing stage; Stage III, the crack propagation stage; Stage IV, the damage stage; and Stage V, the post-peak stage.

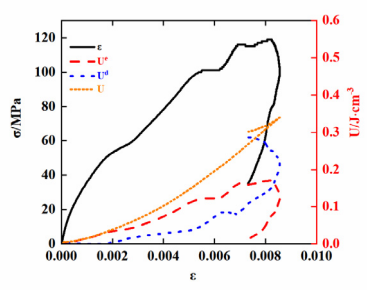

0°, 0 MPa

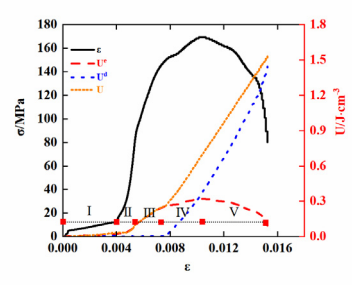

0°, 12.5 MPa

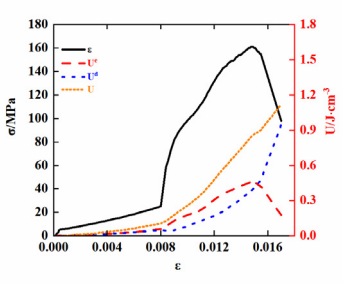

0°, 25 MPa

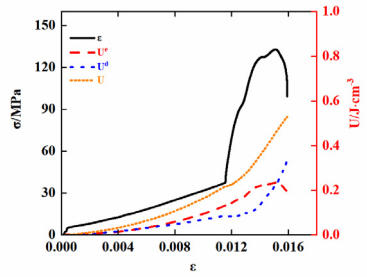

0°, 37.5 MPa

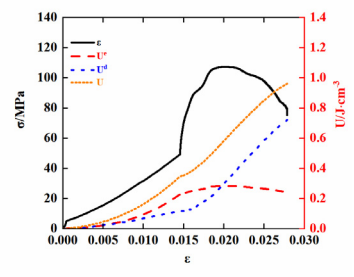

0°, 50 MPa

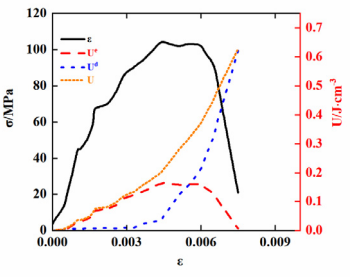

30°, 0 MPa

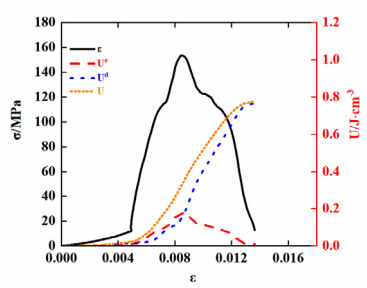

30°, 12.5 MPa

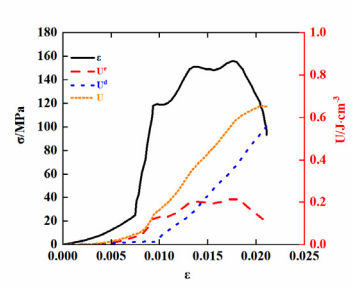

30°, 25 MPa

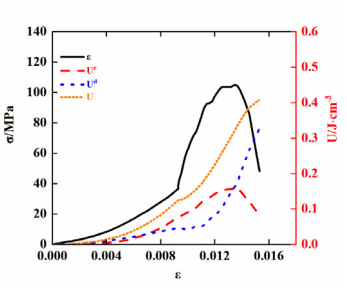

30°, 37.5 MPa

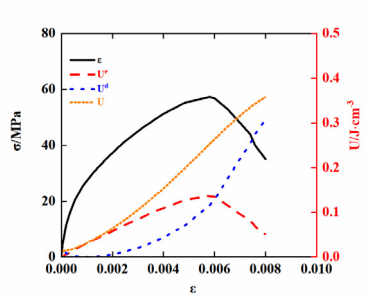

45°, 0 MPa

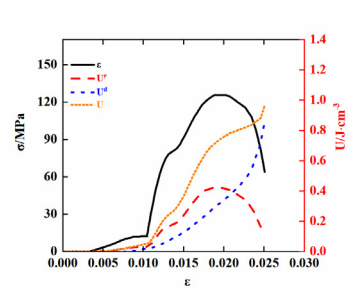

45°, 12.5 MPa

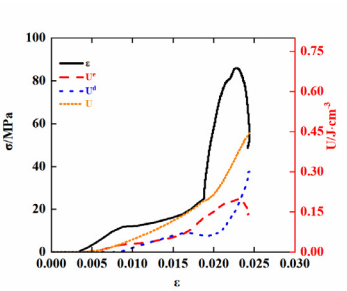

45°, 25 MPa

Figure 5. *Cont.*

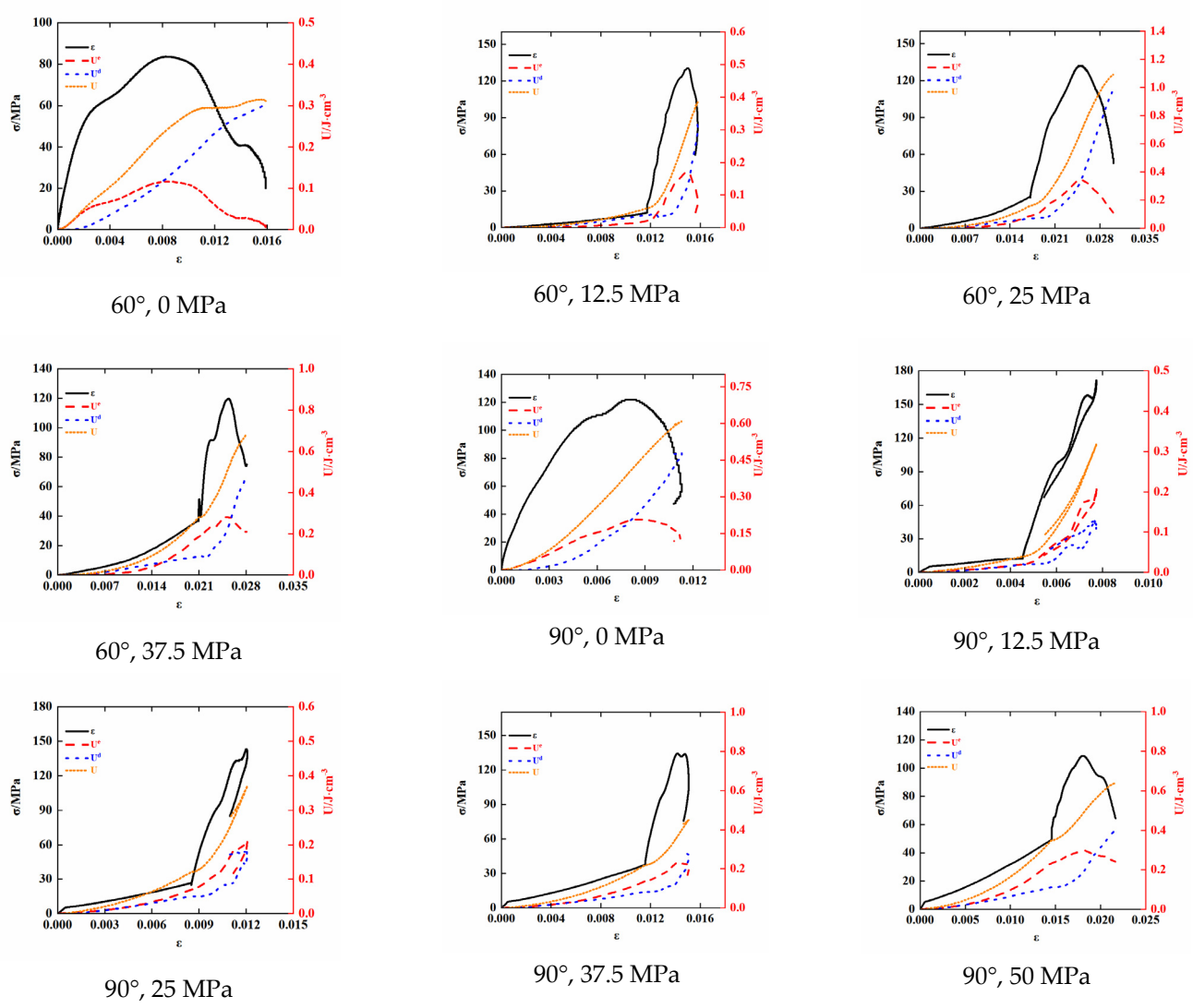

Figure 5. Global energy evolution characteristics of sandstone.

Figure 5 illustrates the distinct global energy evolution of sandstone under varying prestress and different bedding angles. Moreover, a notable contrast is evident between the global energy evolution of sandstone. Thus, this study delves into the global energy evolution characteristics of sandstone separately from the perspectives of prestress and bedding.

Stage I: During this stage, as the prestress elevates from 0 MPa to 50 MPa, the static loading phase extends, leading to a significant surge in the energy stored within the rock mass. This emphasizes the pivotal impact of prestress on the energy evolution characteristics of sandstone. The process of static loading allows the energy input in the sandstone, driven by prestressing, to steadily accumulate, causing a continuous rise in each energy parameter of the sandstone. It is important to note that this stage is absent in the global energy evolution of sandstone when solely subjected to pure dynamic loading tests. Additionally, the bedding angle also plays a substantial role in shaping the static load energy evolution stage of sandstone. As the bedding angle increases, the energy stored in the sandstone initially rises before eventually decreasing. This phenomenon is attributed to the alteration in mechanical response and energy distribution within the sandstone as the bedding angle increases. Notably, when the bedding angle is 0° or 90°, the sandstone exhibits higher strength and lower energy accumulation, whereas at the 30°, 45° and 60° bedding angles, the sandstone displays lower strength and a gradual increase in energy accumulation.

Stage II: This phase demonstrates the joint influence of prestress and bedding angle on the global energy evolution of sandstone. Moreover, as static and dynamic loads increase, the energy of sandstone under various bedding angles and prestresses gradually rises. Elastic energy predominates during this stage, attributed to the elastic deformation of sandstone. Furthermore, as the prestress increases, the deformation of sandstone gradually shifts from elastic to dissipative, potentially due to the varying degrees of deterioration within the sandstone as prestress intensifies. Consequently, prestress exerts a notable impact on the internal structure of sandstone, significantly shaping the global energy evolution characteristics. The influence of bedding angle on the energy evolution of sandstone in this stage is comparatively minor. Therefore, emphasis should be placed on comprehending the effect of prestressing on the energy evolution law of sandstone during this stage.

Stage III: During this phase, elastic energy continues to dominate the energy consumption. This can be attributed to the fact that despite some fracture expansion in sandstone at this stage, the accumulated elastic energy from the early stages of static and dynamic load combinations remains the primary contributor. Furthermore, both prestress and bedding angle have minimal influence on the energy evolution of sandstone during this phase.

Stage IV: The damage stage. Similar to Stage III, elastic energy continues to be the primary contributor to energy consumption during this phase. The presence of fracture expansion in the rock sample at this stage does not significantly alter the dominance of accumulated elastic energy from the previous stages. Consequently, elastic energy remains the dominant factor in energy consumption. Moreover, prestress and bedding angle exhibit minimal influence on the energy evolution of sandstone in this stage.

Stage V: Post-peak stage. In this phase, as strain increases, the elastic energy of sandstone under different prestress and bedding angles decreases drastically, while the absorbed and dissipated energy of sandstone experiences a sharp increase. The significant decrease in elastic energy is due to the previous stage where the sandstone undergoes a series of deformation and damage processes, leading to the accumulation of a large amount of elastic energy. However, during the destabilization and damage of sandstone, cracks rapidly expand, causing a sharp increase in dissipative energy and a decrease in elastic energy. In the post-peak phase, the influence of bedding angle and prestress on the energy evolution curve of sandstone is noteworthy. With the increase in prestress, the initial energy value of sandstone rises, consequently affecting the overall shape of the energy evolution curve. Additionally, the initial energy values of sandstone vary with different bedding angles, indicating that the bedding angle also significantly impacts the energy evolution curve of sandstone.

U^e_{ci}, U^e_{cc}, U^e_{cf} and U^e_{cd} represent the elastic energies at the linear elastic point, damage point, peak point and failure point of sandstone, respectively. U^d_{ci}, U^d_{cc}, U^d_{cf} and U^d_{cd} correspondingly denote the dissipated energy of linear elastic point, damage point, peak point and failure point of sandstone; U_{ci}, U_{cc}, U_{cf} and U_{cd} represent the total strain energy of the linear elastic point, damage point, peak point and failure point of sandstone.

The initial prestress and its bedding angle play a crucial role in determining the energy at the elastic points of sandstone. Curves representing these energy parameters at different characteristic points of sandstone under various prestress and bedding angle conditions are presented in Figures 6–9. The analysis results demonstrate that these energy parameters are notably influenced by the initial prestress and bedding angle, highlighting the importance of further examining these effects. Figure 4 illustrates the significant influence of prestress on the energy characteristics of sandstone. As the prestress increases, the degree of deformation in the rock also increases, resulting in higher levels of energy at the elastic points of sandstone. This behavior can be attributed to the fact that prestress acts as an external load, inducing greater strain and stress within the rock, thereby promoting higher deformation, energy accumulation, and dissipation in sandstone. Consequently, the energy characteristics of sandstone exhibit significant variations under different prestress conditions. In addition, the bedding angle also significantly impacts the energy characteristics of sandstone. Notably, when the bedding angle is 45°, the elastic energy at the

elastic points of sandstone is generally at its maximum, whereas sandstones with other bedding angles tend to have lower elastic energy. This observation may be attributed to the alterations in stress distribution and deformation modes within the sandstone due to changes in the bedding angle, consequently affecting the process of energy conversion and dissipation. Additionally, the dissipated energy and total energy at the elastic points of sandstone exhibit fluctuations with the increase in the bedding angle.

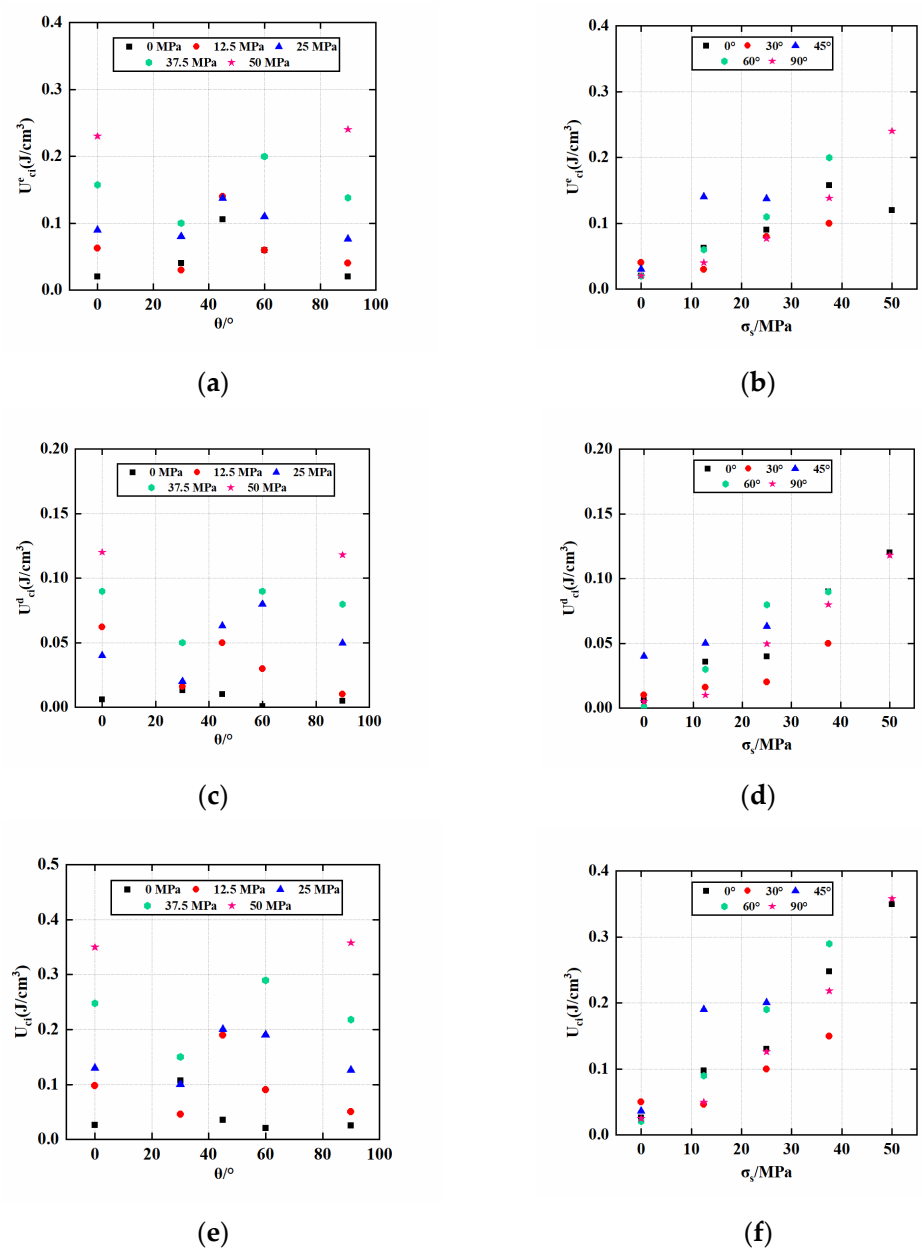

Figure 6. Law of U^{e}_{ci}, U^{d}_{ci}, U_{ci} of sandstone with bedding angle and prestress under different conditions. (**a**) The law of U^{e}_{ci} of sandstone takes the bedding angle as the independent variable; (**b**) the law of U^{e}_{ci} of sandstone takes the prestress as the independent variable; (**c**) the law of U^{d}_{ci} of sandstone takes the bedding angle as the independent variable; (**d**) the law of U^{d}_{ci} of sandstone takes the prestress as the independent variable; (**e**) the law of U_{ci} of sandstone takes the bedding angle as the independent variable; (**f**) the law of U_{ci} of sandstone takes the prestress as the independent variable.

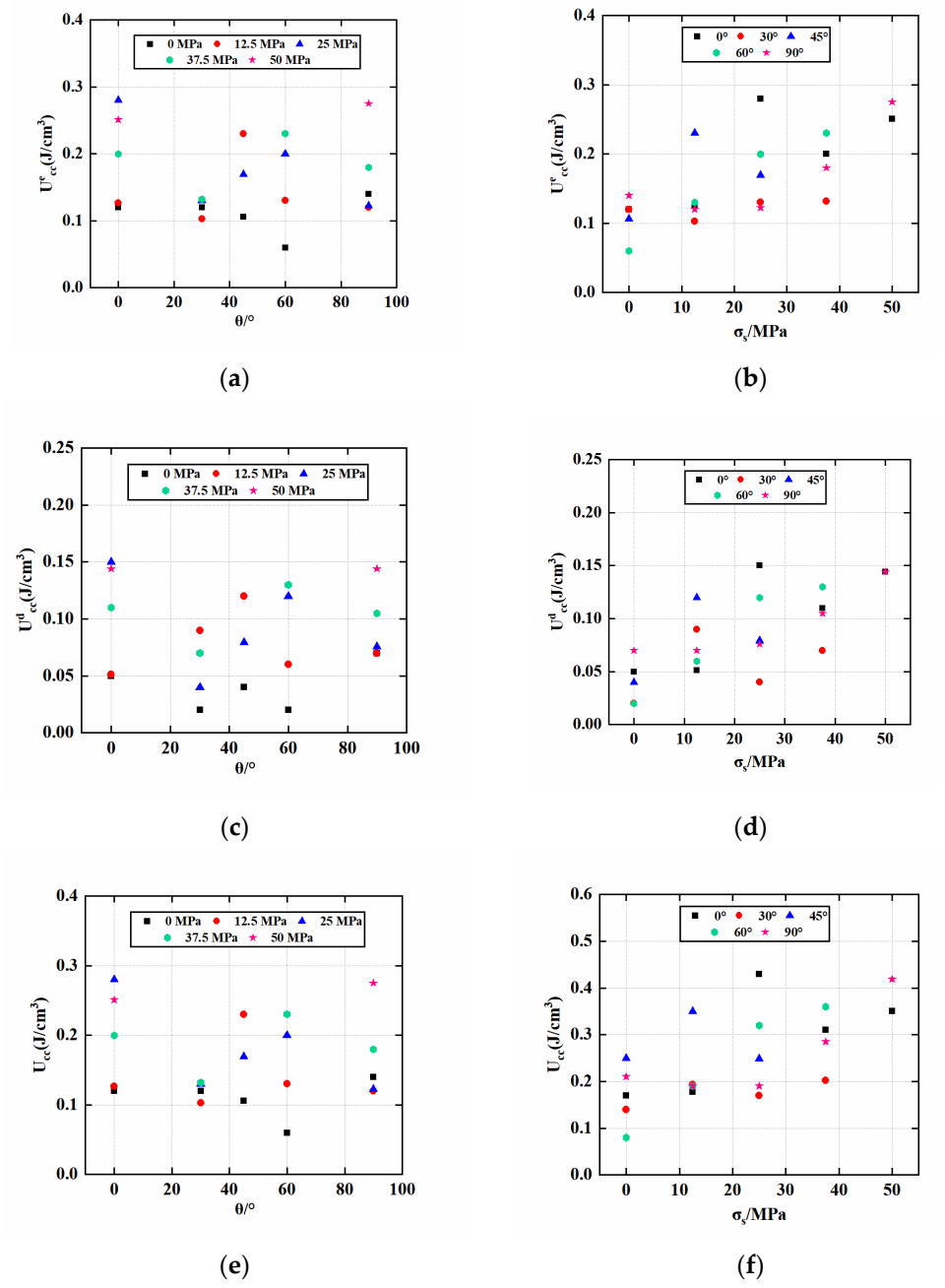

Figure 7. Law of U^e_{cc}, U^d_{cc}, U_{cc} of sandstone with bedding angle and prestress under different conditions. (**a**) The law of U^e_{cc} of sandstone takes the bedding angle as the independent variable; (**b**) the law of U^e_{cc} of sandstone takes the prestress as the independent variable; (**c**) the law of U^d_{cc} of sandstone takes the bedding angle as the independent variable; (**d**) the law of U^d_{cc} of sandstone takes the prestress as the independent variable; (**e**) the law of U_{cc} of sandstone takes the bedding angle as the independent variable; (**f**) the law of U_{cc} of sandstone takes the prestress as the independent variable.

From Figure 7, it is evident that the elastic energy, dissipated energy and total energy at the sandstone damage point increase with the rise in prestress. This behavior can be attributed to the increased prestress causing deformation and strain accumulation in the rock, consequently leading to heightened energy storage and release. Moreover, with the increase in the bedding angle, the elastic energy, dissipative energy and total energy at the sandstone damage point exhibit an initial increase followed by a decrease. This phenomenon may arise from variations in stress distribution and fracture mechanisms in rocks under different bedding angles. At smaller bedding angles, layered sandstone

demonstrates higher strength, leading to enhanced elastic and energy absorption capacity. However, as the bedding angle further increases, the strength of stratified sandstone decreases, resulting in increased fracture propagation and energy release, leading to reduced elastic energy and total energy. These findings offer valuable insights into the energy characteristics of stratified sandstone. As the key controlling factors, prestress and bedding angle significantly influence the energy conversion mechanism of the rock.

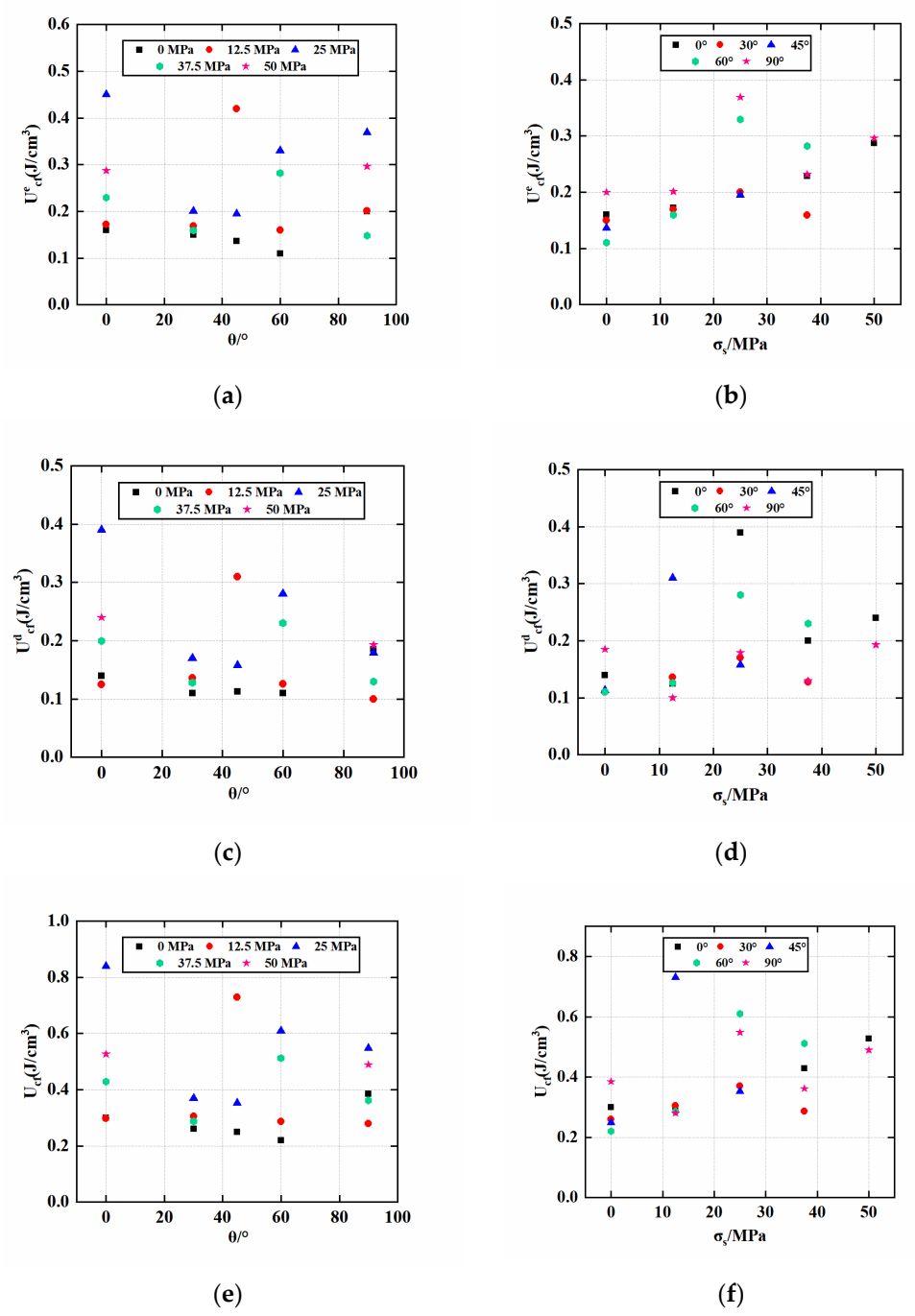

Figure 8. Law of U^e_{cf}, U^d_{cf}, U_{cf} of sandstone with bedding angle and prestress under different conditions. (**a**) The law of U^e_{cf} sandstone takes the bedding angle as the independent variable; (**b**) the law of U^e_{cf} of sandstone takes the prestress as the independent variable; (**c**) the law of U^d_{cf} of sandstone takes the bedding angle as the independent variable; (**d**) the law of U^d_{cf} of sandstone takes the prestress as the independent variable; (**e**) the law of U_{cf} sandstone takes the bedding angle as the independent variable; (**f**) the law of U_{cf} of sandstone takes the prestress as the independent variable.

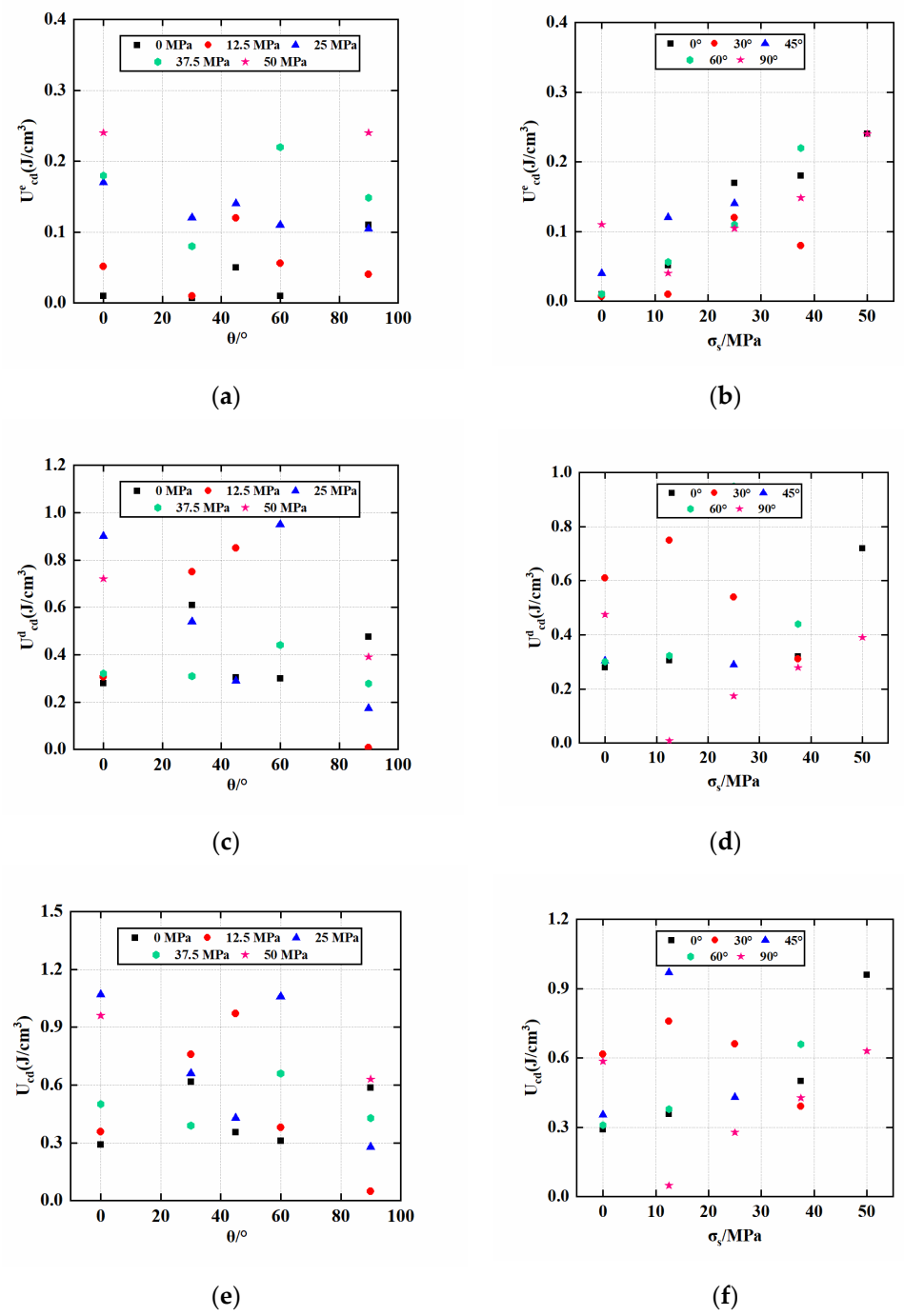

Figure 9. Law of U^{e}_{cd}, U^{d}_{cd}, U_{cd} of sandstone with bedding angle and prestress under different conditions. (**a**) The law of U^{e}_{cd} of sandstone takes the bedding angle as the independent variable; (**b**) the law of U^{e}_{cd} sandstone takes the prestress as the independent variable; (**c**) the law of U^{d}_{cd} sandstone takes the bedding angle as the independent variable; (**d**) the law of U^{d}_{cd} of sandstone takes the prestress as the independent variable; (**e**) the law of U_{cd} of sandstone takes the bedding angle as the independent variable; (**f**) the law of U_{cd} of sandstone takes the prestress as the independent variable.

From Figure 8, it is evident that the elastic energy, dissipative energy, and total energy of sandstone at the peak point increase with the rise in prestress. This indicates a distinct evolution in the energy characteristics of sandstone in response to increasing prestress. Furthermore, the increase in prestress leads to greater deformation of sandstone during the static load stage, resulting in a gradual enhancement of peak energy during the loading process. This phenomenon is likely due to microstructure recombination and

strain accumulation within the rock caused by the increased prestress, leading to greater energy absorption and storage. Moreover, the peak elastic energy, dissipative energy, and total energy of sandstone initially increase and then decrease with the increase in bedding angle. This behavior is linked to changes in the fracture mechanism within the rock due to variations in bedding structure. When the bedding angle is 0° or 90°, the bedding structure may provide additional strength and stiffness, resulting in reduced energy absorption and strain under the same stress. Conversely, at bedding angles of 30°, 45° and 60°, the bedding structure may become unstable, leading to increased crack propagation and energy release, resulting in a gradual increase in the energy signature at the peak point. These observations shed light on the influence of prestress and bedding angle on the energy characteristics of sandstone at the peak point.

From Figure 9, it is evident that the elastic energy of sandstone at the failure point increases with the rise in prestress. This indicates that even under high prestress conditions, where the sandstone becomes unstable and damaged, there is still a certain amount of elastic energy present due to the increased prestress. However, the increase in prestress does not exhibit a clear pattern of influence on the energy dissipation and total energy at the failure point of sandstone. High prestress does not significantly impact the energy dissipation and total energy at the failure point of sandstone. Moreover, the energy of sandstone at the failure point does not exhibit a clear trend with bedding angle. Based on these observations, it appears that the impact of the bedding angle on the energy characteristics of sandstone at the failure point is relatively modest.

5. Evolution Mechanism of Elastic Energy and Dissipative Energy

The increase in prestress introduces changes to the initial state and internal stress distribution of sandstone, thereby influencing the energy conversion and dissipation process during this test under different prestress and bedding angles. On the other hand, variations in bedding angle cause non-uniform stress and strain distribution in sandstone, impacting the mechanism and path of energy conversion. In this section, we analyze the ratio L of elastic energy to dissipated energy and the evolution relationship of strain to delve into the energy conversion mechanism of sandstone under varying prestress and bedding angles. Through studying the correlation between the L value and strain, we can unveil the characteristics and laws governing the energy conversion mechanism of sandstone under this condition.

Figure 10 reveals intriguing insights into the energy conversion mechanism of sandstone under dynamic load conditions. As the sandstone moves from point A to point B, we observe a decrease in the L value for sandstones with bedding angles of 0°, 45°, 60° and 90°, while the L value for the 30° sandstone increases. This behavior can be attributed to the progressive increase in sandstone damage from point A to point B, leading to a corresponding rise in dissipative energy. Consequently, the L value decreases for most sandstone samples, except for the 30° bedding angle, where a dispersed state might influence the L value positively. Similarly, as the sandstone transitions from point B to point C, the L value decreases for all bedding angles (0°, 30°, 45°, 60° and 90°). This reduction is associated with the progressive damage and plastic deformation experienced by the sandstone in this stage. Subsequently, as the sandstone moves from point C to point D, the L value continues to decrease due to the further increase in damage and dissipative energy, culminating in the post-peak rupture stage. Contrary to dynamic loading, the deformation of sandstone under dynamic and static combined loading starts from the static loading point. To investigate the energy conversion mechanism under this condition, this study examines the process from the static loading end. As the sandstone progresses from point a to point b, the L value increases for sandstones with bedding angles of 0°, 45°, 60° and 90°, while remaining consistent with the dynamic load results for other points b to d. In summary, this comprehensive analysis uncovers the complex energy conversion mechanism of sandstone under impact load conditions, providing valuable insights into the influence of prestress and bedding angle on sandstone behavior.

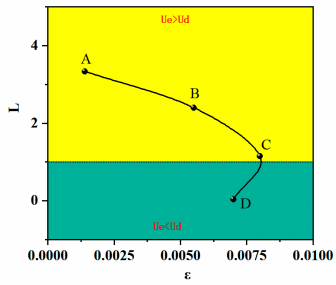

0°, 0 MPa

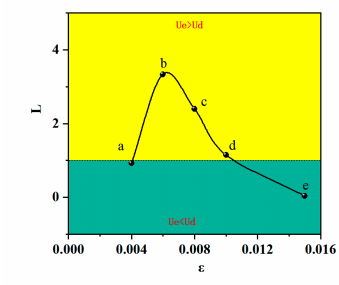

0°, 12.5 MPa

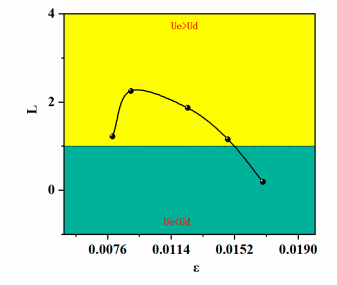

0°, 25 MPa

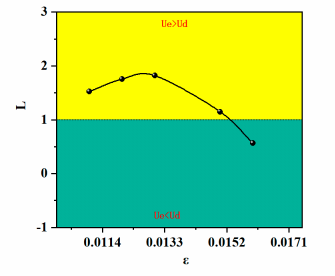

0°, 37.5 MPa

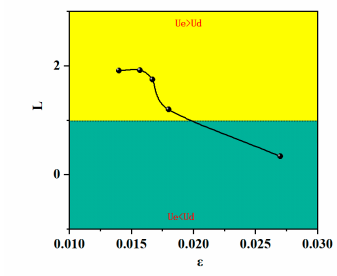

0°, 50 MPa

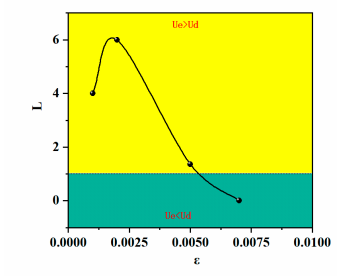

30°, 0 MPa

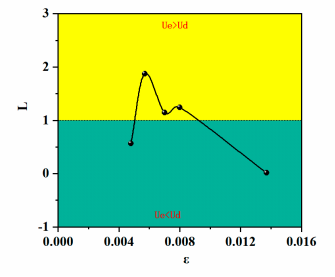

30°, 12.5 MPa

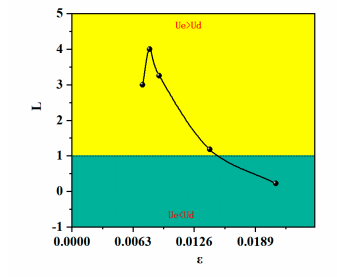

30°, 25 MPa

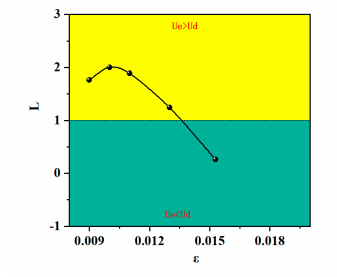

30°, 37.5 MPa

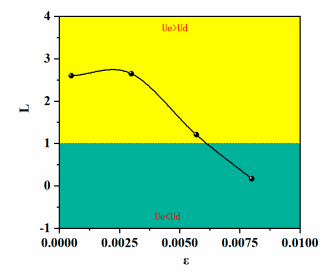

45°, 0 MPa

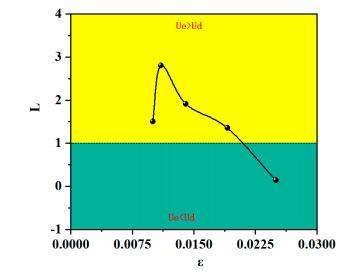

45°, 12.5 MPa

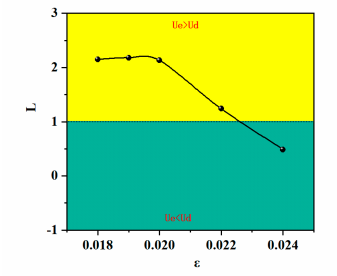

45°, 25 MPa

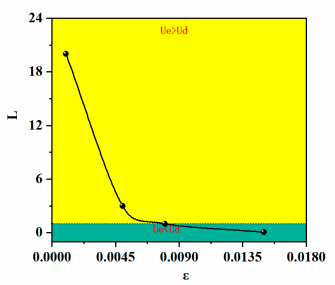

60°, 0 MPa

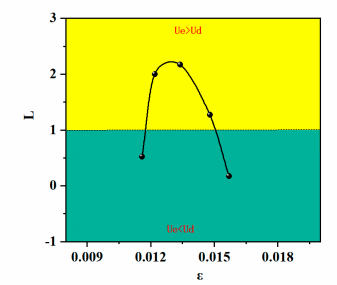

60°, 12.5 MPa

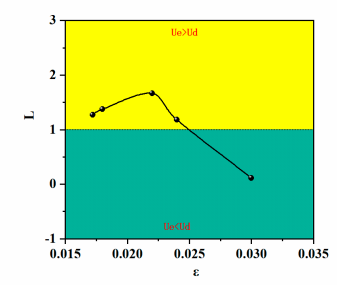

60°, 25 MPa

Figure 10. *Cont.*

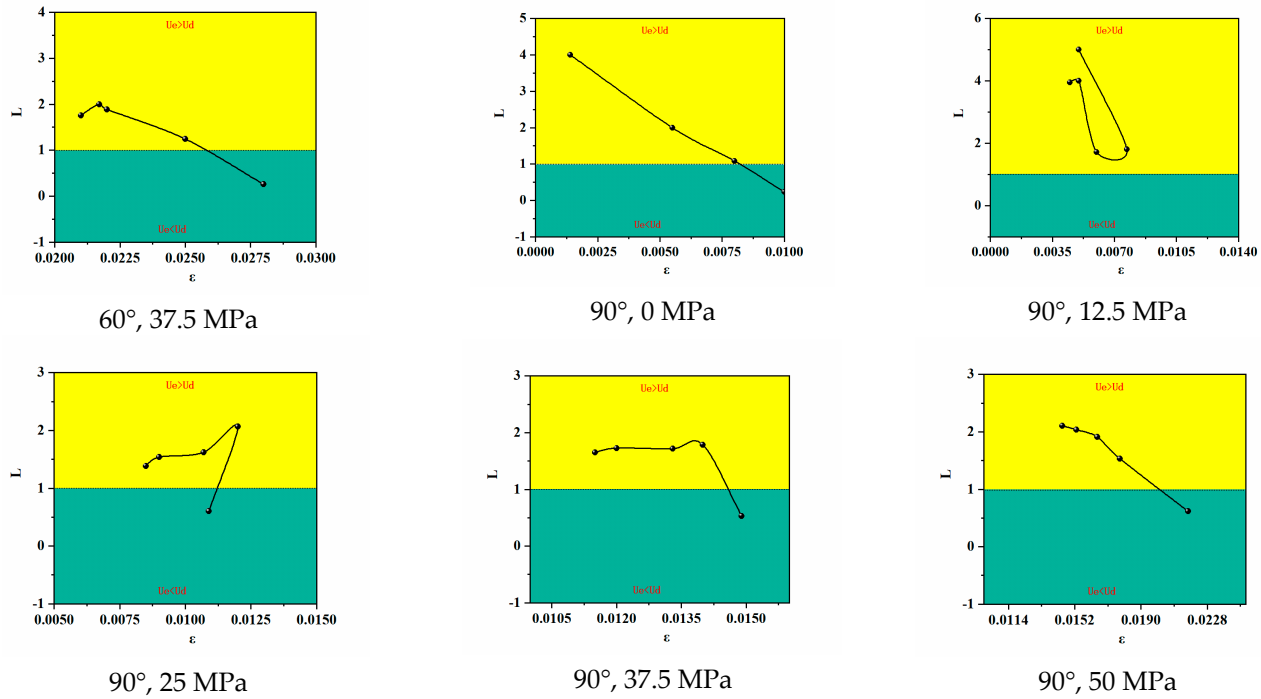

Figure 10. Evolution mechanism of elastic energy and dissipative energy of sandstone.

6. Damage Analysis of Sandstone Caused by Initial Stress and Bedding Angle

6.1. Damage Analysis of Prestressed Sandstone

The damage calculation formula of sandstone under uniaxial compression is as follows:

$$D_1 = U^{\mathrm{d}} / U_s \tag{5}$$

where U^{d} is the dissipated energy of the sandstone under prestress; U_s is the total energy of sandstone under prestress; and D_1 is the damage degree of the sandstone under prestress.

The damage degree within the sandstone varies under different prestress conditions, undergoing processes such as compaction, deformation and damage. To quantitatively assess the degree of damage, the ratio of dissipated energy to total energy of the sandstone is analyzed. Figure 11 illustrates the damage degree curves for different prestressed sandstones with varying bedding angles. The results reveal that sandstone with 30°, 45° and 60° bedding angles exhibits significantly higher initial damage degrees compared to those with 0° and 90° bedding angles. This highlights the considerable influence of bedding angle on the initial damage degree of the sandstone. Changes in the bedding angle can result in alterations in the mechanical behavior and crack development modes in the sandstone, leading to varying degrees of damage. Specifically, at the 0° and 90° bedding angles, the bedding structure may provide additional strength and stiffness, resulting in lower energy absorption and strain under the same stress and, thus, a lower degree of damage. Conversely, at the 30°, 45° and 60° angles, the bedding structure may become unstable, leading to increased crack propagation and energy release, resulting in higher damage to the rock.

6.2. Damage Evolution of Sandstone under Combined Dynamic and Static Loading

Building upon the previous research, the failure process of sandstone under prestress and bedding angles involves energy conversion. During loading, external energy is introduced into the rock, leading to destruction through various forms of energy conversion. In this paper, we employ the ratio of dissipative energy to the total energy of sandstone as the chosen damage variable. The calculation formula for sandstone under different prestress and bedding angles is as follows:

$$D_2 = \frac{U^d{}_s}{U} = \frac{\int_{\varepsilon_0}^{\varepsilon_1} \sigma_1 d\varepsilon - \frac{1}{2E_u}\sigma_1^2}{\int_{\varepsilon_0}^{\varepsilon_1} \sigma_1 d\varepsilon} \quad (6)$$

where $U^d{}_s$ and U represent the dissipated energy and total energy of sandstone in this test.

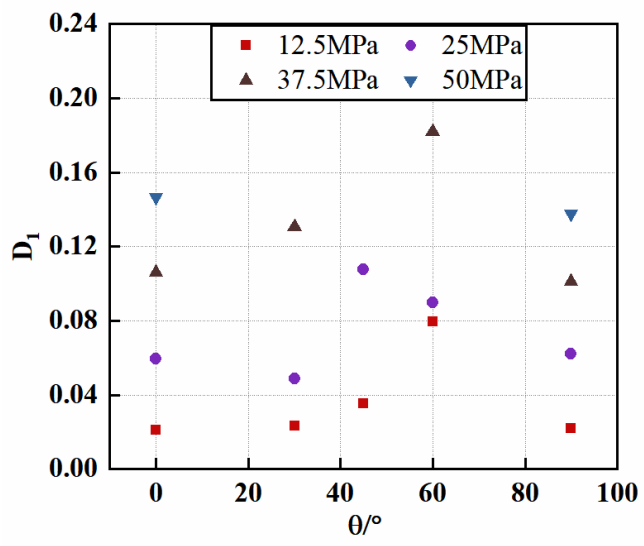

Figure 11. Curves of sandstone static load damage degree and bedding angle under different conditions.

By employing the defined damage variables and utilizing the calculation formula mentioned above, we can quantitatively assess the degree of damage within the sandstone. This provides an objective approach to evaluate the sandstone failure process and facilitates comparisons and analyses with other studies. The careful selection of these damage variables is crucial for a comprehensive understanding of the mechanical behavior and failure mechanism of sandstone. It enables us to gain insights into the energy conversion and distribution within rocks during loading, as well as the accumulation and evolution of damage. Through this examination of variables, we can uncover the mechanical response and damage mechanism of sandstone, thereby furnishing more accurate information and a solid foundation for rock engineering design, geological disaster prediction and resource exploitation.

In this experimental study, sandstone specimens are subjected to static loading with varying initial prestresses. The damage observed in the sandstone is a result of the combined effects of the initial static loading and dynamic and static loading. The initial prestress contributes to the damage value of the sandstone, denoted as D_1. Subsequently, the overall damage experienced by the sandstone under the dynamic and static combined loading is represented by the coupling damage value, referred to as D_{coupling}:

$$D_{\text{coupling}} = D_1 + (1 - D_1)D_2 \quad (7)$$

Utilizing the formula provided earlier, the author has plotted the coupled damage curves of sandstone under various prestress and bedding angle conditions, as illustrated in Figure 12.

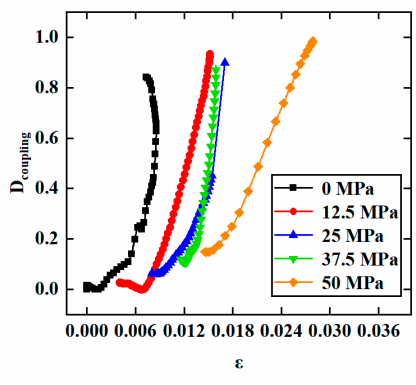

0°

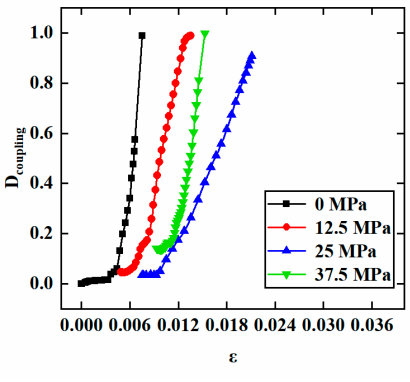

30°

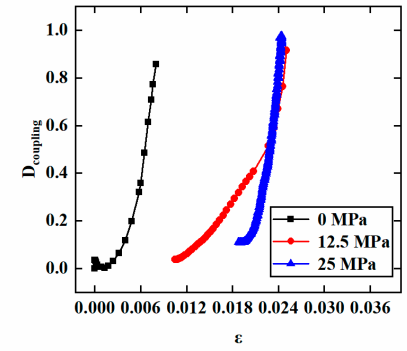

45°

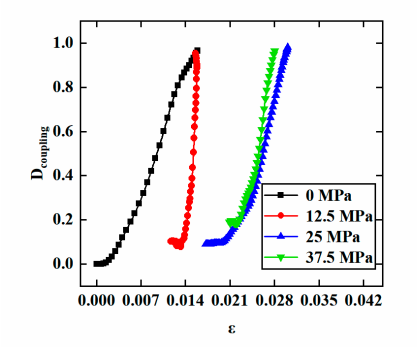

60°

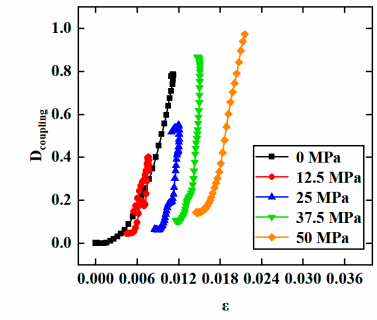

90°

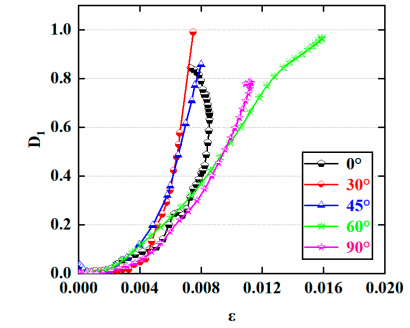

0 MPa

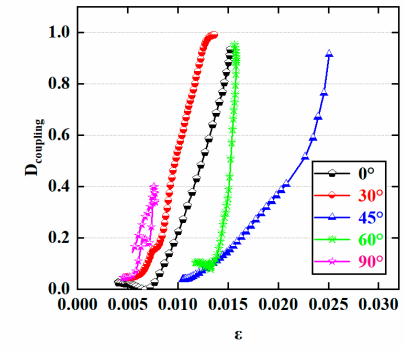

12.5 MPa

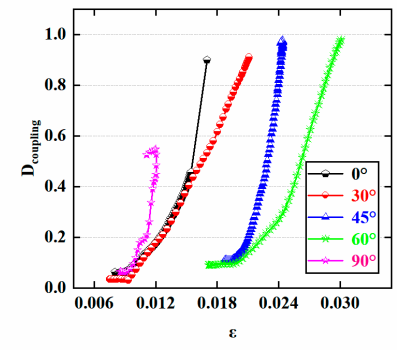

25 MPa

Figure 12. *Cont.*

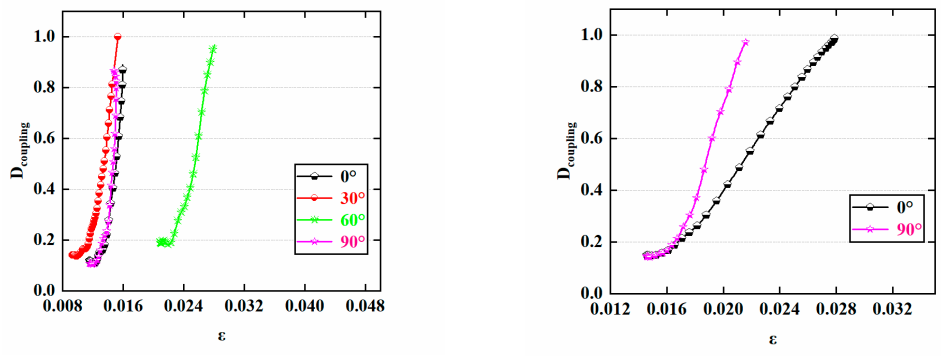

Figure 12. Damage evolution characteristics of sandstone.

Based on the observations from Figure 12, the combined damage mechanism curves of sandstone under varying prestress and bedding angles demonstrate a two-stage pattern. In the initial stage, the coupling damage of sandstone increases gradually with strain, while in the latter stage, the coupling damage accelerates rapidly with strain. This two-stage characteristic indicates the complexity of sandstone's deformation and failure process, with significant damage accumulation during deformation. Furthermore, the damage curve of sandstone is notably affected by prestress. The coupling damage curves of sandstone show notable variations under different prestressed conditions. As the prestress increases, the first stage duration of the coupled damage curve decreases, suggesting that higher prestress levels lead to an increased initial damage degree in sandstone, hastening its approach to the peak stress state. This demonstrates the considerable influence of prestress on sandstone's damage behavior, rendering it more susceptible to damage. Additionally, the bedding angle also affects the coupled damage curve of sandstone. For instance, under 12.5 MPa prestress, the coupled damage curve of sandstone at a 90° angle exhibits a rebound effect. This phenomenon underscores the significant influence of bedding angle on sandstone's coupled damage behavior, shedding light on the role of bedding structure in rock deformation and failure.

The figure also illustrates how both prestress and bedding angle impact the initial damage of sandstone. As prestress increases, the initial damage point of sandstone coupling damage rises, indicating a gradual escalation in the initial damage degree. This phenomenon can be attributed to the intensified crack propagation within the sandstone under higher prestress, resulting in a greater degree of damage. Higher prestress renders the sandstone more susceptible to stress concentration and failure during loading. Moreover, the initial damage degrees of sandstones with different bedding angles exhibit significant variations. This disparity can be attributed to distinct internal rock structures and crack distributions corresponding to different bedding angles. The varying layered structures with differing inclinations might lead to distinct crack propagation paths and mechanical behaviors, thus generating different initial damage degrees during loading. These results demonstrate the critical influence of bedding angle on the rock's damage characteristics and underscore the key role of bedding structure in shaping these characteristics. The insights gained from this research offer a deeper understanding of how prestress and bedding angle affect the initial damage of sandstone, holding great significance for rock engineering design, geological hazard assessment and resource exploitation. Moreover, for underground engineering and energy development, this in-depth understanding of sandstone's initial damage characteristics provides valuable guidance for engineering design and risk assessment, enabling more precise and informed decision making.

7. Conclusions

As a result of the study, it is found that prestress and bedding angle have important effects on the energy conversion mechanism and damage mechanism of sandstone. The research findings are expected to reveal vital insights into the energy dissipation and damage mechanisms of sandstone under various prestress and bedding angle conditions. Some detailed conclusions are as follows:

1. The global energy evolution curve and damage mechanism evolution curve of sandstone under prestress and bedding inclination were obtained.
2. With the increase in prestress, the energy of each characteristic point of sandstone increases, and the total energy evolution curve changes. In addition, the energy of each characteristic point of sandstone is also different with different bedding angles.
3. It is found that the energy conversion mechanism of sandstone is also different under different loading modes.
4. It is found that the prestress is positively correlated with the initial damage degree of sandstone, and the initial damage degree of sandstone with different bedding angles is also different.

Author Contributions: W.F.: Original draft preparation. J.Z.: Acquisition of financial support for project leadership. Y.Y.: Formal analysis. K.F. and Y.X.: Data curation. S.W.: Software. All authors have read and agreed to the published version of the manuscript.

Funding: This study was supported by the National Natural Science Foundation of China (Grant Nos. 52034009 and 51974319), the National Key R&D Program of China (No. 2022YFC3004602) and the Yue Qi Distinguished Scholar Project (Grant No. 2020JCB01). The authors would like to thank shiyanjia lab (www.shiyanjia.com, accessed on 1 June 2023) for the support of the SEM test.

Data Availability Statement: Data available on request from the authors.

Conflicts of Interest: The authors declare no conflict of interest.

References

1. Wang, P.; Xu, J.; Fang, X.; Wang, P. Energy dissipation and damage evolution analyses for the dynamic compression failure process of red-sandstone after freeze-thaw cycles. *Eng. Geol.* **2017**, *221*, 104–113. [CrossRef]
2. Li, D.; Han, Z.; Zhu, Q.; Zhang, Y.; Ranjith, P.G. Stress wave propagation and dynamic behavior of red sandstone with single bonded planar joint at various angles. *Int. J. Rock Mech. Min. Sci.* **2019**, *117*, 162–170. [CrossRef]
3. Hao, X.; Du, W.; Zhao, Y.; Sun, Z.; Zhang, Q.; Wang, S.; Qiao, H. Dynamic tensile behaviour and crack propagation of coal under coupled static-dynamic loading. *Int. J. Min. Sci. Technol.* **2020**, *30*, 659–668. [CrossRef]
4. Su, Q.; Ma, Q.; Ma, D.; Yuan, P. Dynamic mechanical characteristic and fracture evolution mechanism of deep roadway sandstone containing weakly filled joints with various angles. *Int. J. Rock Mech. Min. Sci.* **2021**, *137*, 104552. [CrossRef]
5. Li, X.; Wang, S.; Xia, K.; Tong, T. Dynamic Tensile Response of a Microwave Damaged Granitic Rock. *Exp. Mech.* **2020**, *61*, 461–468. [CrossRef]
6. Qi, C.; Wang, M.; Qian, Q. Strain-rate effects on the strength and fragmentation size of rocks. *Int. J. Impact Eng.* **2009**, *36*, 1355–1364. [CrossRef]
7. Xu, Y.; Dai, F.; Du, H. Experimental and numerical studies on compression-shear behaviors of brittle rocks subjected to combined static-dynamic loading. *Int. J. Mech. Sci.* **2020**, *175*, 105520. [CrossRef]
8. Zhang, J.; Fan, W.; Yang, Y.; Zhang, Y.; Dong, X.; Xing, Y.; Zeng, W.; Fang, K. Dynamic response and energy evolution of sandstone under combined dynamic and static loading. *Soil Dyn. Earthq. Eng.* **2023**, *174*, 108168. [CrossRef]
9. Fan, W.; Zhang, J.; Yang, Y.; Zhang, Y.; Dong, X.; Xing, Y. Study on the Mechanical Behavior and Constitutive Model of Layered Sandstone under Triaxial Dynamic Loading. *Mathematics* **2023**, *11*, 1959. [CrossRef]
10. Fan, W.; Zhang, J.; Niu, W.; Zhang, Y.; Dong, X.; Xing, Y.; Zeng, W. Study on dynamic loading characteristics and energy evolution of sandstone with double cracks. *Theor. Appl. Fract. Mech.* **2023**, *125*, 103893. [CrossRef]
11. Khayrutdinov, M.M.; Kongar-Syuryun, C.B.; Khayrutdinov, A.M.; Tyulyaeva, Y.S. Improving safety when extracting water-soluble ores by optimizing the parameters of the backfill mass. *Bezop. Tr. V Promyshlennosti* **2021**, *2021*, 53–59. [CrossRef]
12. Adigamov, A.E.; Yudenkov, A.V. Stress-strain behavior model of disturbed rock mass with regard to anisotropy and discontinuities. *Min. Inf. Anal. Bull.* **2021**, *8*, 93–103. [CrossRef]
13. Rybak, J.M.; Kongar-Syuryun, C.; Tyulyaeva, Y.; Khayrutdinov, A.M.; Akinshin, I. Geomechanical substantiation of parameters of technology for mining salt deposits with a backfill. *Min. Sci.* **2021**, *28*, 19–32. [CrossRef]

14. Kongar-Syuryun, C.; Ubysz, A.; Faradzhov, V. Models and algorithms of choice of development technology of deposits when selecting the composition of the backfilling mixture. *IOP Conf. Ser. Earth Environ. Sci.* **2021**, *684*, 012008. [CrossRef]
15. Chang, X.; Zhang, X.; Qian, L.Z.; Chen, S.H.; Yu, J. Influence of bedding anisotropy on the dynamic fracture behavior of layered phyllite. *Eng. Fract. Mech.* **2022**, *260*, 108183. [CrossRef]
16. Zhao, Y.; Sun, Z.; Gao, Y.; Wang, X.; Song, H. Influence of bedding planes on fracture characteristics of coal under mode II loading. *Theor. Appl. Fract. Mech.* **2022**, *117*, 103131. [CrossRef]
17. Zhang, X.; Ou, X.; Gong, F.; Yang, J. Effects of Bedding on The Dynamic Compressive Properties of Low Anisotropy Slate. *Rock Mech. Rock Eng.* **2018**, *52*, 981–990. [CrossRef]
18. Ye, H.; Li, X.; Lei, T.; Li, L.; Wang, Q.; Li, N. Dynamic response characteristics and damage rule of graphite ore rock under different strain rates. *Sci. Rep.* **2023**, *13*, 2151. [CrossRef]
19. Wu, H.; Fan, A.; Zheng, Z.; Wang, M.; Li, S.; Zhang, B.; Liu, Y. Dynamic mechanical properties and failure behaviors of brittle rock materials with a tunnel-shaped opening subjected to impact loads. *J. Mater. Res. Technol.* **2023**, *25*, 3285–3297. [CrossRef]
20. Lu, A.; Chang, X.; Hu, S.; Xia, Y.; Li, M.; Zhang, H. Impact of Moisture Content on the Brittle-Ductile Transition and Microstructure of Sandstone under Dynamic Loading Conditions. *Adv. Civ. Eng.* **2021**, *2021*, 6690171. [CrossRef]
21. Liu, D.; Li, D.; Zhao, F.; Wang, C. Fragmentation characteristics analysis of sandstone fragments based on impact rockburst test. *J. Rock Mech. Geotech. Eng.* **2014**, *6*, 251–256. [CrossRef]
22. Cen, D.; Huang, D.; Song, Y.; Jiang, Q. Direct Tensile Behavior of Limestone and Sandstone with Bedding Planes at Different Strain Rates. *Rock Mech. Rock Eng.* **2020**, *53*, 2643–2651. [CrossRef]
23. Cen, D.; Li, Y.; Huang, D. Mechanical behavior of the weak bedding plane within sandstone subjected to dynamic load of cyclic tension. *Bull. Eng. Geol. Environ.* **2022**, *81*, 424. [CrossRef]
24. Zhou, T.; Zhu, J.; Xie, H. Mechanical and Volumetric Fracturing Behaviour of Three-Dimensional Printing Rock-like Samples Under Dynamic Loading. *Rock Mech. Rock Eng.* **2020**, *53*, 2855–2864. [CrossRef]
25. Wu, N.; Zhang, C.; Maimaitiyusupu, S.; Zhu, Z. Investigation on Properties of Rock Joint in Compression Dynamic Test. *KSCE J. Civ. Eng.* **2019**, *23*, 3854–3863. [CrossRef]
26. Yan, Z.; Dai, F.; Zhu, J.; Xu, Y. Dynamic Cracking Behaviors and Energy Evolution of Multi-flawed Rocks Under Static Pre-compression. *Rock Mech. Rock Eng.* **2021**, *54*, 5117–5139. [CrossRef]
27. Yan, Z.; Dai, F.; Liu, Y.; Du, H. Experimental investigations of the dynamic mechanical properties and fracturing behavior of cracked rocks under dynamic loading. *Bull. Eng. Geol. Environ.* **2020**, *79*, 5535–5552. [CrossRef]
28. Li, P.; Cai, M.; Gao, Y.; Guo, Q.; Miao, S.; Ren, F.; Wang, Y. Mechanical responses and fracturing behavior of jointed rock masses with a cavity under different dynamic loads. *Int. J. Impact Eng.* **2023**, *178*, 104608. [CrossRef]
29. Li, C.; Xu, Y.; Chen, P.; Li, H.; Lou, P. Dynamic Mechanical Properties and Fragment Fractal Characteristics of Fractured Coal–Rock-Like Combined Bodies in Split Hopkinson Pressure Bar Tests. *Nat. Resour. Res.* **2020**, *29*, 3179–3195. [CrossRef]
30. Tao, M.; Zhao, H.; Li, X.; Li, X.; Du, K. Failure characteristics and stress distribution of pre-stressed rock specimen with circular cavity subjected to dynamic loading. *Tunn. Undergr. Space Technol.* **2018**, *81*, 1–15. [CrossRef]
31. Chang, S.; Xu, J.Y.; Bai, E.L.; Zheng, G.H.; Lv, X.C. Static and dynamic mechanical properties and deterioration of bedding sandstone subjected to freeze-thaw cycles: Considering bedding structure effect. *Sci. Rep.* **2020**, *10*, 12790. [CrossRef] [PubMed]
32. Wang, W.; Wang, H.; Li, D.; Li, H.; Liu, Z. Strength and Failure Characteristics of Natural and Water-Saturated Coal Specimens under Static and Dynamic Loads. *Shock Vib.* **2018**, *2018*, 3526121. [CrossRef]
33. Zhou, Z.; Cai, X.; Li, X.; Cao, W.; Du, X. Dynamic Response and Energy Evolution of Sandstone Under Coupled Static–Dynamic Compression: Insights from Experimental Study into Deep Rock Engineering Applications. *Rock Mech. Rock Eng.* **2019**, *53*, 1305–1331. [CrossRef]
34. Li, Y.; Peng, J.; Zhang, F.; Qiu, Z. Cracking behavior and mechanism of sandstone containing a pre-cut hole under combined static and dynamic loading. *Eng. Geol.* **2016**, *213*, 64–73. [CrossRef]
35. Cai, X.; Zhou, Z.; Du, X. Water-induced variations in dynamic behavior and failure characteristics of sandstone subjected to simulated geo-stress. *Int. J. Rock Mech. Min. Sci.* **2020**, *130*, 104339. [CrossRef]
36. Ke, B.; Zhang, J.; Deng, H.; Yang, X. Dynamic Characteristics of Sandstone under Coupled Static-Dynamic Loads after Freeze-Thaw Cycles. *Appl. Sci.* **2020**, *10*, 3351. [CrossRef]
37. Du, H.-B.; Dai, F.; Liu, Y.; Xu, Y.; Wei, M.-D. Dynamic response and failure mechanism of hydrostatically pressurized rocks subjected to high loading rate impacting. *Soil Dyn. Earthq. Eng.* **2020**, *129*, 105927. [CrossRef]
38. Du, H.-b.; Dai, F.; Xu, Y.; Yan, Z.; Wei, M.-d. Mechanical responses and failure mechanism of hydrostatically pressurized rocks under combined compression-shear impacting. *Int. J. Mech. Sci.* **2020**, *165*, 105219. [CrossRef]
39. Zhu, Q.; Li, D.; Han, Z.; Xiao, P.; Li, B. Failure characteristics of brittle rock containing two rectangular holes under uniaxial compression and coupled static-dynamic loads. *Acta Geotech.* **2021**, *17*, 131–152. [CrossRef]
40. Xue, W.; Mao, X.; Xu, W.; Zhang, H.; Gao, C. Macro-and meso-scale study on dynamic mechanical properties of shaft lining concrete exposed to high water pressure. *Case Stud. Constr. Mater.* **2022**, *17*, e01502. [CrossRef]
41. Zhao, G.; Zhang, L.; Dai, B.; Liu, Y.; Zhang, Z.; Luo, X. Experimental Investigation of Pre-Flawed Rocks under Dynamic Loading: Insights from Fracturing Characteristics and Energy Evolution. *Materials* **2022**, *15*, 8920. [CrossRef] [PubMed]

42. Zhou, Y.; Sheng, Q.; Li, N.; Fu, X. The Influence of Strain Rate on the Energy Characteristics and Damage Evolution of Rock Materials Under Dynamic Uniaxial Compression. *Rock Mech. Rock Eng.* **2020**, *53*, 3823–3834. [CrossRef]
43. Fan, W.; Zhang, J.; Dong, X.; Zhang, Y.; Yang, Y.; Zeng, W.; Wang, S. Fractal dimension and energy-damage evolution of deep-bedded sandstone under one-dimensional dynamic and static combined loading. *Geomech. Geophys. Geo-Energy Geo-Resour.* **2022**, *8*, 177. [CrossRef]